Heterozygosity for *Roquin*^{san} leads to angioimmunoblastic T-cell lymphoma-like tumors in mice

Julia I. Ellyard,[1] Tiongsun Chia,[1] Socorro-Maria Rodriguez-Pinilla,[2] Jaime L. Martin,[1] Xin Hu,[1] Manuel Navarro-Gonzalez,[3] Juan F. Garcia,[4] Marie-Helene Delfau-Larue,[5] Santiago Montes-Moreno,[6] Philippe Gaulard,[7] Matthew C. Cook,[8] Giles Walters,[3] *Miguel A. Piris,[9] and *Carola G. Vinuesa[1]

[1]Department of Pathogens and Immunity, John Curtin School of Medical Research, Australian National University, Canberra, Australia; [2]Pathology Department, Fundacion Jimenez Diaz, Madrid, Spain; [3]Renal Department, Canberra Hospital, Canberra, Australia; [4]Pathology Department, MD Anderson Cancer Center, Madrid, Spain; [5]Inserm U955, Université Paris Est, Créteil, France; Assistance Publique–Hôpitaux de Paris (AP-HP); Immunologie Biologique, Hôpital Henri Mondor, Créteil, France; [6]Lymphoma Group, Spanish National Cancer Research Center, Madrid, Spain; [7]Inserm U955, Université Paris Est, AP-HP, and Département de Pathologie, Hôpital Henri Mondor, Créteil, France; [8]Immunology Department, Canberra Hospital, Canberra, Australia; and [9]Jefe de Servicio de Anatomía Patológica, Hospital Universitario Marques de Valdecilla, Santander, Spain

Angioimmunoblastic T-cell lymphoma (AITL) is the second most common peripheral T-cell lymphoma with unusual clinical and pathologic features and a poor prognosis despite intensive chemotherapy. Recent studies have suggested AITL derives from follicular helper T (T_{FH}) cells, but the causative molecular pathways remain largely unknown. Here we show that approximately 50% of mice heterozygous for the "*san*" allele of *Roquin* develop tumors accompanied by hypergammaglobulinemia by 6 months of age. Affected lymph nodes displayed the histologic features diagnostic of AITL, except for the presence of expanded FDC networks. Accumulation of T_{FH} cells preceded tumor development, and clonal rearrangements in the TCR-β genes were present in most tumors. Furthermore, T_{FH} cells exhibited increased clonality compared with non-T_{FH} cells from the same lymph nodes, even in the absence of tumors. Genetic manipulations that prevent T_{FH} development, such as deletion of ICOS, CD28, and SAP, partially or completely abrogated tumor development, confirming a T_{FH}-derived origin. Roquin$^{san/+}$ mice emerge as a useful model to investigate the molecular pathogenesis of AITL and for preclinical testing of therapies aimed at targeting dysregulated T_{FH} cells or their consequences. (*Blood*. 2012; 120(4):812-821)

Introduction

Angioimmunoblastic T-cell lymphoma (AITL) is a distinct subtype of peripheral T-cell lymphoma, displaying autoimmune features and poor prognosis.[1-3] Unlike other tumors in which morbidity and mortality occur as a consequence of complications of tumor growth, AITL-associated mortality is thought to be a consequence of profound immune dysregulation.[4,5] AITL disease outcome is poor, with an overall 7-year survival rate of 30%,[3] and patients usually do not respond well to cytotoxic chemotherapeutic treatment.

AITL is more common in elderly patients, with a median age of 64 years.[6] Patients commonly present with lymphadenopathy, hepatosplenomegaly, skin rash, fever, hemolytic anemia, and hypergammaglobulinemia.[7,8] Histologic features of AITL typically include effacement of the lymph node architecture, prominent arborization of endothelial venules, and an expanded extrafollicular meshwork of follicular dendritic cells (FDCs).

The neoplastic T cells account for only a small fraction of the lymphoid infiltrate and are admixed with a large number of reactive immune cell types, including small lymphocytes, eosinophils, histiocytes, plasma cells, and abnormal B cells often infected with EBV.[3] Indeed, close to 90% of the gene expression signature is contributed by nonneoplastic cells[9] and characterized by expression of many genes associated with the tumor microenvironment, including genes expressed by B cells, FDCs, chemokines, the extracellular matrix, and the vascular system.[9] In addition, AITL has a gene expression profile analogous to that of activated $CD4^+$ helper T cells but not of $CD8^+$ T cells.[10] It is enriched for expression of follicular helper T (T_{FH}) cell signature genes, including expression of *CXCL13, BCL6*, and *PD1*[9,10] (17284527; 16625095). These findings, together with the identification of T_{FH} markers in tumor tissues sections by immunohistochemistry,[11-14] have suggested that T_{FH} cells are the neoplastic cells in AITL.[10] However, the molecular mechanisms that drive T_{FH} neoplastic transformation remain largely unknown.

To date, there are no mouse models available of this human disease, which hampers both elucidation of pathogenic pathways and the possibility of undertaking preclinical trials using compounds targeting T_{FH} cells. We have previously reported the characterization of the *sanroque* mouse strain that bears a homozygous point mutation in the *Roquin/Rc3h1* gene,[15] and the resulting allele is designated *Roquin*^{san}. ROQUIN has previously been shown to bind *Icos* mRNA through its ROQ domain and regulate inducible T-cell costimulator (ICOS) mRNA stability.[16-18] Mutant ROQUIN encoded by *Roquin*^{san} binds *Icos* mRNA with higher affinity, leading to slower mRNA decay. In *Roquin*$^{san/san}$ mice, aberrant expression of ICOS on $CD4^+$ T cells contributes to an excessive accumulation of T_{FH} cells,[15,17,19] which in turn causes

Submitted July 17, 2011; accepted June 2, 2012. Prepublished online as *Blood* First Edition paper, June 13, 2012; DOI 10.1182/blood-2011-07-365130.

*M.A.P and C.G.V. contributed equally to this study.

The online version of this article contains a data supplement.

The publication costs of this article were defrayed in part by page charge payment. Therefore, and solely to indicate this fact, this article is hereby marked "advertisement" in accordance with 18 USC section 1734.

lupus-like disease characterized by lymphadenopathy, splenomegaly, hypergammaglobulinemia, and the development of glomerulonephritis.[15] Interestingly, mice heterozygous for the *Roquin "san"* allele (*Roquin*$^{san/+}$) also have dysregulated T_{FH} cells but do not develop the full-blown lupus-like autoimmunity. Instead, a proportion of mice develop asymmetric lymphadenopathy.

Here we report that enlarged lymph nodes from *Roquin*$^{san/+}$ mice display T-cell oligoclonality and many histopathologic features consistent with human AITL. Furthermore, tumor development was found to be dependent on T_{FH} cells, suggesting that, as in human AITL, T_{FH} cells may be the neoplastic driver of disease. These findings suggest that *Roquin*$^{san/+}$ mice may provide a good model for human AITL and thereby promote further understanding of disease mechanisms and help in the discovery of novel therapeutic targets.

Methods

Mice and tumor characterization

Roquin$^{san/+}$, *Roquin*$^{san/+}$*Sap*$^{-/-}$, *Roquin*$^{san/+}$*Cd28*$^{-/-}$, and *Roquin*$^{san/+}$ *Icos*$^{-/-}$ mice were bred and maintained under pathogen-free conditions at the Animal Bioscience Services facility. All experimental procedures were carried out in compliance with protocols approved by the Australian National University Animal Ethics and Experimentation Committee. Lymph nodes examined for tumor development were cervical nodes, axillary nodes, brachial nodes, and inguinal nodes. Size of lymph nodes was visually inspected and classified as tumorous when they were at least 5 times the size of normal lymph nodes from wild-type mice. Mice were characterized as tumorous if there was at least 1 enlarged lymph node among the aforementioned inspected nodes.

Antibodies

All antibodies and streptavidin conjugates used for flow cytometry were from BD Biosciences unless otherwise indicated: anti–mouse B220 PECy7, B220 PerCP, CD4 APC Cy7, CD4 APC, CD8 FITC, CXCR5-biotin, GL-7 FITC, FAS PE, and PD-1 PE (eBioscience), mouse anti-Bcl6 A647, streptavidin PerCP Cy5.5, and streptavidin PE Cy7. For immunohistochemistry, the primary antibodies used were goat anti–mouse CD3ϵ (Santa Cruz Biotechnology), goat anti–mouse Pax-5 (Santa Cruz Biotechnology), and rat anti–mouse F4/80 (BMA Biomedicals).

ELISA

ELISA was performed to analyze total IgG levels in mouse serum as previously described.[20]

Histology and immunohistochemistry

Hematoxylin and eosin-stained sections from a series of 19 *Roquin*$^{san/+}$ and 4 *Roquin*$^{san/san}$ formalin-fixed, paraffin-embedded lymph nodes were morphologically reviewed. Five lymph nodes belonging to *Roquin*$^{+/+}$ littermates were examined as controls. Immunohistochemistry for mouse CD3ϵ, Pax5, and F4/80 was performed on formalin-fixed, paraffin-embedded sections as follows: tissue sections were deparaffinized, rehydrated, and treated for antigen retrieval. After quenching of endogenous peroxidase and blocking in normal serum, tissues were incubated with primary antibody overnight at 4°C, followed by incubation with biotinylated secondary antibody. Specific interactions were visualized using the Envision System (Dako North America) following the manufacturer's instructions. Slides were counterstained with hematoxylin, dehydrated, and mounted. Slides were visualized on a Leica DMD108 microsystem at 25°C and acquired with LAS-DMD Version 1.3.1 software (Leica).

Flow cytometry

Single-cell suspensions of lymph nodes were prepared in FACS buffer (PBS/2% BSA/0.05% NaN_3) by sieving and gently pipetting through 70-μm nylon mesh filters. After red blood cell lysis, 3×10^6 cells were incubated with each antibody or conjugate layer for 30 to 60 minutes on ice. Samples were run on a FACSCalibur (BD Biosciences). Analysis was performed using FlowJo Version 7.2.5 (TreeStar).

B- and T-cell clonality studies

PCR was performed to analyze the clonal expansion of T and B cells.[21] DNA was extracted from paraffin sections, and T-cell and B-cell clonal expansion was detected by analysis of TCR-β, TCR-γ, and IgH gene rearrangement. TCR-β gene clonality was assayed at V-DJ and D-J rearrangements in 4 different PCR reactions (Vβ-Jβ1, Vβ-Jβ2, dβ1-Jβ1, Dβ2-Jβ2) as previously described.[22] The TCR-γ gene clonality was assayed at V-J rearrangements in 1 PCR (Vγ4-Jγ1) using Vγ4 and Jγ1 consensus primers previously described by Kawamoto et al.[23] The IgH gene clonality at D-J rearrangements in 1 PCR (DSF-JH4), using DSF and JH4 consensus primers previously described by Kawamoto et al.[23] PCR primers (Jβ1, Jβ2, Jγ1, and JH4), were labeled at the 5′end with 6-Fam for GeneScanning of the PCR products. The fluorochrome-labeled single-strand (denatured) PCR products were analyzed by capillary electrophoresis using the ABI PRISM 3700 Genetic Analyser and Gene Scan Version 1.2 software (Applied Biosystems).[24] Appropriate positive and negative controls were included in all experiments.

For repertoire analyses of purified T cells, T_{FH} ($CD4^+CXCR5^+PD\text{-}1^{hi}$) and non-$T_{FH}$ ($CD4^+CXCR5^-PD\text{-}1^{lo}$) cell subsets were purified by FACS sorting on a FACSDIVA (BD Biosciences), and RNA was isolated using an RNAqueous-Micro Kit (Ambion) according to the manufacturer's instructions. TCRV-β repertoires were measured using real-time PCR on the Biorad iCycler. One PCR for each Vβ family (22 reactions) was performed in triplicate for each sample to cover the repertoire. Threshold cycles were converted to a percentage mRNA signal presuming a 100% efficiency reaction. For clonal analysis within each Vβ family, the PCR product was amplified with standard PCR using FAM-labeled Vβ constant region reverse primer for 6 to 10 cycles and run on a high-resolution sequencing gel to delineate CDR3 spectratypes.

Loss of heterozygosity

Using flow cytometry, 1, 10, or 100 T_{FH} and naive T cells were sorted directly into the wells of a 96-well plate and digested with proteinase K (QIAGEN) to isolate DNA. A primary PCR was performed for the region of *Roquin* approximately 200 bp either side of the *san* mutation. A secondary PCR was performed using fluorescently labeled primers to detect the *Roquin*^{san} and *Roquin*$^{+}$ alleles, as regularly used to genotype the *sanroque* mouse strain. Primer sequences are available on request.

Statistics

Statistical analysis was performed in Prism Version 5 software (GraphPad Software) with a Mann-Whitney test unless otherwise stated.

Results

Roquin$^{san/+}$ mice develop asymmetrically enlarged lymph nodes and hypergammaglubulinemia

We have previously reported that *Roquin*$^{san/san}$ mice develop generalized lymphadenopathy, splenomegaly, and T_{FH} dysregulation.[15] In these mice, accumulation of T_{FH} cells causes a lupus-like pathology.[20] Initial inspection of *Roquin*$^{san/san}$ lymph node histopathology showed large polymorphic infiltrates and the presence of atypical T cells characteristic of human AITL (Figure 1). Given that reactive nodes commonly accompany systemic autoimmunity and this may confound the diagnosis of AITL, we investigated heterozygous *Roquin*$^{san/+}$ mice instead: initial observations suggested that a proportion *Roquin*$^{san/+}$ mice developed lymphadenopthy in the absence of overt autoimmunity.

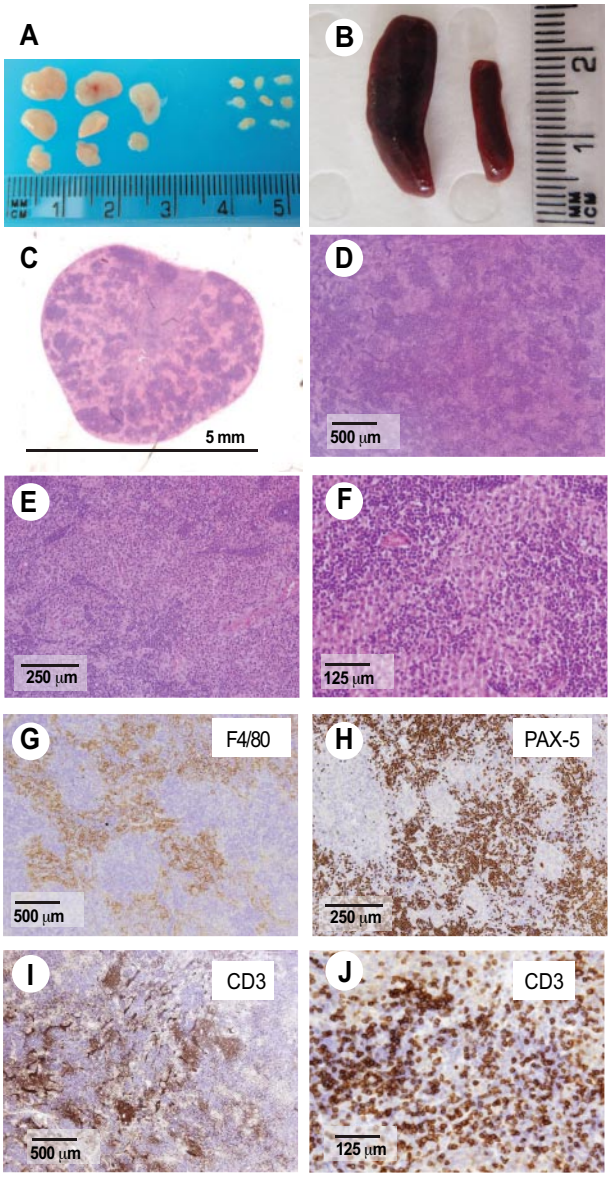

Figure 1. AITL-like pathology in *Roquin*$^{san/san}$ mice. (A-B) *Roquin*$^{san/san}$ mice develop generalized lymphadenopathy (A) and splenomegaly compared with *Roquin*$^{+/+}$ littermate controls (B). Lymph node sections were stained with hematoxylin and eosin (C-F) or antibodies to the macrophage marker F4/80 (G), B-cell marker pax-5 (H), or the pan-T-cell marker CD3ϵ (I-J). Enlarged lymph nodes are characterized by a polymorphic infiltrate containing plasma cells (E), macrophages (F-G), and atypical T cells sometimes forming a rosetta pattern characteristic of AITL (J). Pictures are representative of 4 mice analyzed, all 26 to 40 weeks of age.

To assess lymph node pathology in *Roquin*$^{san/+}$ mice, groups of mice were killed at monthly intervals from 4 months of age. All the major lymph nodes, including cervical, axillary, brachial, and inguinal, were examined. None of the *Roquin*$^{san/+}$ mice developed the generalized symmetric lymph node enlargement that is observed in 100% of *Roquin*$^{san/san}$ mice by 8 weeks of age. Instead, 53% of mice (100 of 188 mice studied) developed 1 to 4 enlarged lymph nodes, whereas other lymph nodes remained normal (Figure 2A; Table 1). This lymphadenopathy was not lethal, with affected mice able to live to more than 1 year (data not shown). From here on, these enlarged lymph nodes are referred to as tumor lymph nodes.

Cellularity was increased by 50- to 150-fold in tumor lymph nodes. Generally, a tumor lymph node consisted of 5.0×10^7 to 1.5×10^8 cells, whereas the normal lymph node in the same mouse or in *Roquin*$^{san/+}$ mice without tumors consisted of approximately 1.0×10^6 cells (data not shown). The prevalence of tumors was 1.6 times higher in female mice (65%) than in male mice (41%; $P = .001$) regardless of age (Table 1). The sex distribution ratio for human AITL cases has been reported to be 1:1.[25,26]

Although the age of onset could not be accurately determined because of the tumors only being externally palpable once they had reached a considerable size, 4 of 11 mice (36%) investigated at 4 to 5 months of age had already developed tumors, suggesting some tumors are likely to develop before 4 months of age.

In addition to lymphadenopathy, many AITL patients present with splenomegaly.[7,8] *Roquin*$^{san/+}$ mice displayed a slight but significant ($P < .05$) increase in spleen weight compared with control *Roquin*$^{+/+}$ mice (Figure 2B-C). No significant difference in spleen size was observed between *Roquin*$^{san/+}$ mice with or without tumors, suggesting that splenomegaly does not correlate with, and may precede, lymphadenopathy. This is consistent with observations that nontumor lymph nodes from *Roquin*$^{san/+}$ mice are often

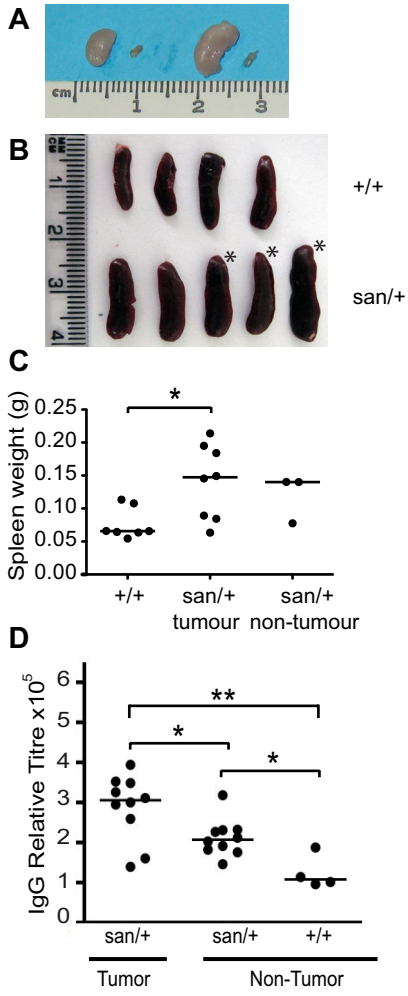

Figure 2. Roquin$^{san/+}$ mouse develop asymmetric lymphoadenopathy and splenomegaly. (A) Comparison of enlarged cervical and inguinal lymph nodes with the contralateral normal lymph node in a *Roquin*$^{san/+}$ female mouse. (B) Representative diagram of spleens from 5 *Roquin*$^{san/+}$ and 4 *Roquin*$^{+/+}$ control age-matched mice. *Mice with lymphadenopathy. (C) Spleen weights of *Roquin*$^{san/+}$ mice separated into those with and without lymphadenopathy compared with *Roquin*$^{+/+}$ controls. Mice were 18 to 40 weeks of age. (D) Total serum IgG titres assayed by ELISA. *Roquin*$^{san/+}$ mice with lymph node tumors have a statistically significant increase in serum IgG titres compared with nontumor *Roquin*$^{san/+}$ mice: $*P < .05$; $**P < .01$.

Table 1. Tumor incidence in *Roquin*$^{san/+}$ mice

Age, mo	Male, no. (%)	Female, no. (%)	Total, no. (%)
4-5	ND	4/11 (36)	4/11 (36)
6	14/36 (39)	12/19 (63)	26/55 (47)
7	9/20 (45)	29/38 (76)	38/58 (66)
8-15	15/36 (42)	17/28 (61)	32/64 (50)
Total	38/92 (41)	62/96 (65)	100/188 (53)

Female sex bias: $\chi^2 = .001$.
ND indicates not determined.

larger than lymph nodes from *Roquin*$^{+/+}$ control mice (data not shown).

Hypergammaglobulinemia is another frequent finding in AITL, with 50% of patients displaying increased IgG in the serum.[3,6] Interestingly, although 4-month-old *Roquin*$^{san/+}$ mice do not develop overt lupus-like autoimmunity, *Roquin*$^{san/+}$ mice, both with and without tumors, developed hypergammaglobulinemia, showing that total serum IgG levels increased 2- to 3-fold above *Roquin*$^{+/+}$ mice (Figure 2D). A moderate (1.5-fold) but statistically significant ($P < .05$) increase in total serum IgG was observed in *Roquin*$^{san/+}$ mice that had developed tumors compared with mice of the same genetic background without tumors. Investigation of serum IgG levels over time suggested that, even at 6 weeks of age, Roquin$^{san/+}$ mice exhibit increased serum IgG titers compared with age-matched controls; however, this did not reach significance until 15 weeks of age (supplemental Figure 1, available on the *Blood* Web site; see the Supplemental Materials link at the top of the online article).

Histopathology of Roquin$^{san/+}$ lymph nodes is reminiscent of AITL

Diagnosis of AITL is based on histologic analysis. The 5 main diagnostic criteria consist of: (1) effaced lymph node architecture, (2) prominent arborization of epithelioid venules, (3) extrafollicular meshwork of FDCs, (4) presence of atypical T cells with T_{FH} phenotype, and (5) scattered large CD20$^+$ B cells.[3] Histopathologic examination of hematoxylin and eosin-stained sections of enlarged lymph nodes from Roquin$^{san/+}$ mice showed features reminiscent of AITL, including effacement of the nodal architecture, prominent vascularization, atypical T cells, and large B cells (Figure 3).

In addition to these features, there was a striking increase in the number of macrophages within the paracortex as shown by F4/80 staining with occasional foci of myeloid metaplasia (Figure 3B). Dense aggregates of small PAX5-positive lymphocytes were visible all over the parenchyma forming follicles without germinal centers (GCs), although a few large pale lymphoid cells were always found among them (Figure 3C-D). The same reactive B-blasts were also found in the interfollicular areas of the lymph node. Small clusters of mature plasma cells were also seen. A polymorphic infiltrate composed of small- to medium-sized proliferating CD3-positive lymphocytes was found in the interfollicular compartment, some of them showing cytologic atypica and increased size (Figure 3E). Moreover, occasionally T cells formed rosettes around large blasts (Figure 3F), which have been reported in AITL. Sinusoidal dilatation was also evident, as well as vessels filled with T cells. A prominent feature present in most AITL cases, but absent in the tumors of *Roquin*$^{san/+}$ mice, is prominent expansion of the FDC network,[3,7,8,27] as determined by an absence of CD21$^+$ dendritic cells in lymph node sections (data not shown). Together, this histologic appearance is highly reminiscent of AITL.

In contrast, histologic examination of nonenlarged lymph nodes from tumor-bearing *Roquin*$^{san/+}$ mice revealed that nodal architecture was preserved (Figure 3G). These lymph nodes displayed both primary and secondary follicles with reactive GCs as well as a marked increase of mature plasma cells in the interfollicular area (Figure 3H).

Analysis of tumor composition

In AITL, the neoplastic T cells account for only a small fraction of the lymphoid infiltrate and are admixed with a large number of reactive immune cell types, including small lymphocytes, eosinophils, histiocytes, plasma cells, and large B cells. To quantify tumor composition, we enumerated T, B, and myeloid cells subsets by flow cytometry.

There was a significantly increased proportion of B cells in tumor lymph nodes compared with normal lymph nodes from either *Roquin*$^{san/+}$ or *Roquin*$^{+/+}$ mice (Figure 4A). Analysis of T_{FH} cells revealed that the frequency of these cells was increased in "normal" Roquin$^{san/+}$ lymph nodes compared with wild-type *Roquin*$^{+/+}$ mice (Figure 4B,D-E), and this was accompanied by a significant increase in frequency of GC B cells (Figure 4C). In contrast, the tumor lymph node displayed frequencies similar to *Roquin*$^{+/+}$ mice. Comparing an enlarged tumor node with its contralateral nonenlarged lymph node, although the proportion of T_{FH} cells identified as either PD-1^{hi}CXCR5$^+$ (Figure 4B; $P < .001$)

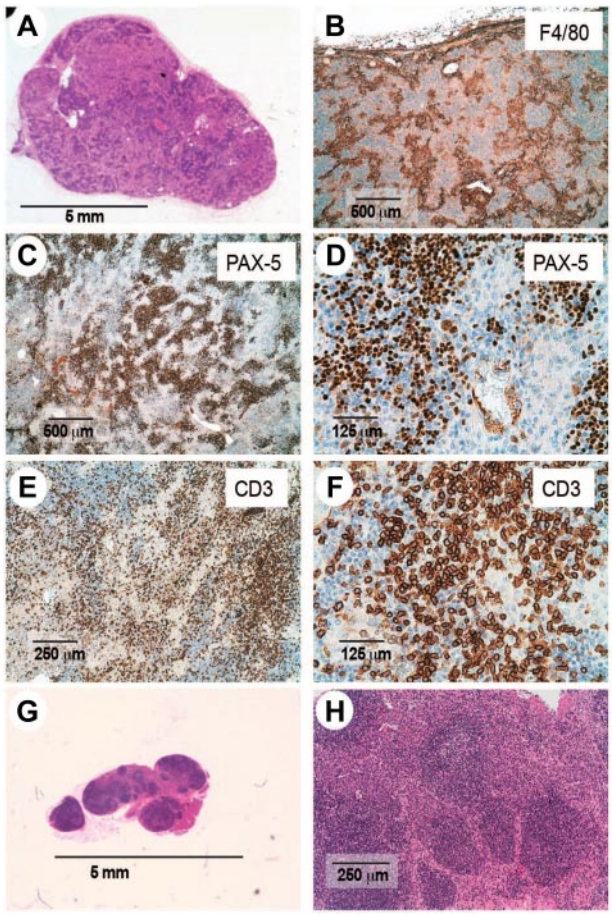

Figure 3. Histologic examination of enlarged lymph nodes from *Roquin*$^{san/+}$ mice. Sections from enlarged (A-F) or nonenlarged lymph nodes (G-H) were stained with hematoxylin and eosin (A,G-H) or antibodies to the macrophage marker F4/80 (B), B-cell marker pax-5 (C-D), or pan-T-cell marker CD3ε (E-F). Sections are representative of 19 mice analyzed. All mice are 26 to 40 weeks of age.

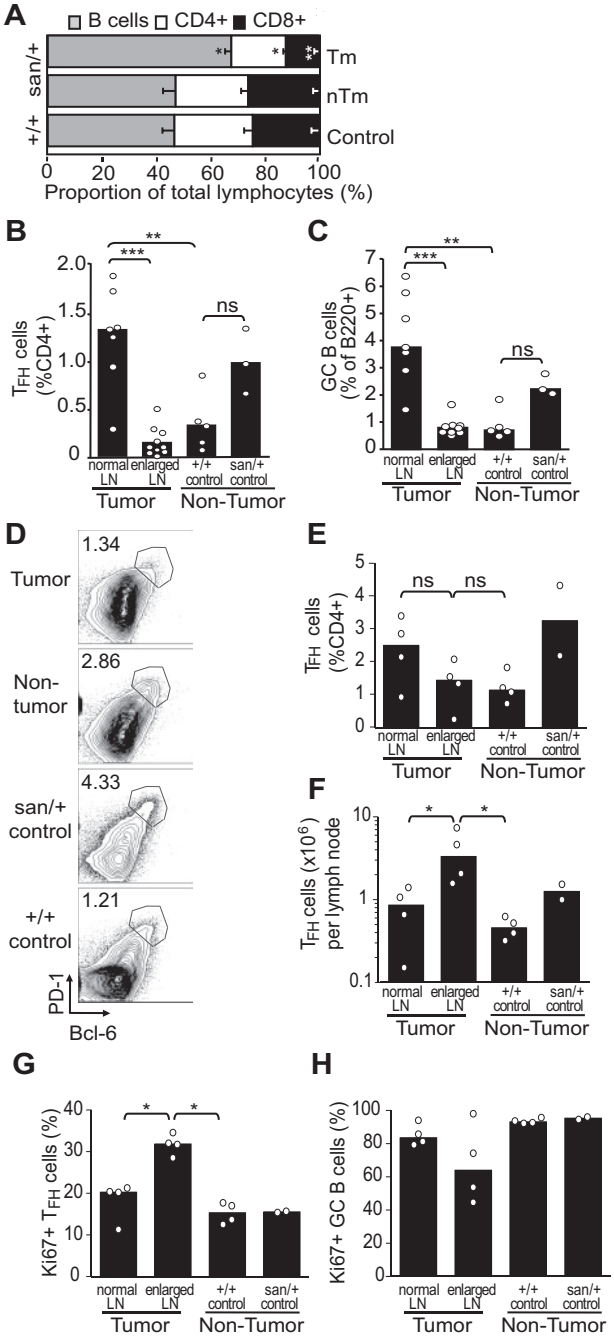

Figure 4. Cellular composition of tumor lymph nodes from *Roquin*$^{san/+}$ mice. Frequency of cellular subsets as measured by flow cytometry. (A) Lymphocyte composition of tumor (Tm) and nontumor (nTm) lymph nodes from *Roquin*$^{san/+}$ and *Roquin*$^{+/+}$mice. (B-C) Percentage of T_{FH} ($CD4^+PD\text{-}1^{hi}CXCR5^+$) and GC B ($B220^+FAS^+GL7^{hi}$) cells in enlarged (tumor) and nonenlarged (normal) lymph nodes from *Roquin*$^{san/+}$ mice compared with control *Roquin*$^{san/+}$ and *Roquin*$^{+/+}$mice. (D) Representative FACS plots showing the percentage of T_{FH} based on $CD4^+PD\text{-}1^{hi}Bcl\text{-}6^+$ cells in tumor, nontumor lymph nodes compared with normal *Roquin*$^{san/+}$ mice. (E-F) Comparison of T_{FH} cells ($CD4^+PD\text{-}1^{hi}Bcl\text{-}6^+$), frequency (as $\%CD4^+$), and total numbers in tumor and contralateral nontumor lymph nodes compared with lymph nodes from normal *Roquin*$^{san/+}$ mice. (G-H) Proportions of T_{FH} (G) and GC B cells (H) undergoing proliferation, as indicated by expression of Ki-67. Histograms in all panels show the mean with SEM (A) or median (B-H) values of 2 to 10 mice 26 to 40 weeks of age. Results are representative of at least 2 independent experiments. ns indicates not significant. $^*P < .05$; $^{**}P < .01$; $^{***}P < .001$.

or $PD\text{-}1^{hi}Bcl\text{-}6^+$ (Figure 4D-E; not significant) within $CD4^+$ T cells was decreased, the total T_{FH}-cell number was significantly increased (Figure 4F; $P < .05$). This supports the hypothesis that, in tumor lymph nodes, an initial expansion of T_{FH} cells is diluted because of a large reactive infiltrate resulting in lymphadenopathy. This is also consistent with the observation that T_{FH} cells contribute to only a small fraction of the cellularity of human AITL-affected lymph nodes.[9,10] Analysis of expression of the proliferation marker, Ki-67, by flow cytometry indicated that approximately 30% the T_{FH} cells in the tumor lymph nodes of *Roquin*$^{san/+}$ mice were proliferating (Figure 4G). This was significantly higher ($P < .05$) than the proportion of proliferating T_{FH} cells in either the nontumor lymph node from tumor-bearing *Roquin*$^{san/+}$ mice or lymph nodes from *Roquin*$^{+/+}$ mice. These results are also consistent with the abnormal $CD3\epsilon^+$ proliferating cells observed in the histologic sections (Figure 3E). In contrast, GC B cells in the tumor lymph node appeared to be less proliferative compared with both the *Roquin*$^{san/+}$ and *Roquin*$^{+/+}$ controls (Figure 4H), although the differences were not significant.

An increased frequency of myeloid cells and dendritic cells was also detected by flow cytometry (Figure 5A), with monocyte-derived dendritic cells being the most dysregulated subset with a 2- to 3-fold expansion ($P = .0535$) in the tumor lymph node compared with wild-type mice (Figure 5B). Monocyte-derived dendritic cells were expanded to an intermediate level ($P = .1099$) in the contralateral nontumor lymph nodes (Figure 5A-B). In contrast, $CD8^+$ and $CD8^-$ dendritic cells were proportionally decreased, significantly and nonsignificantly, respectively, in both tumor and nontumor lymph nodes from *Roquin*$^{san/+}$ mice (Figure 5B).

Together, these data suggest that dysregulation of T_{FH} cells and subsequent GC expansion are an obligatory consequence of the *Roquin*^{san} mutation and preclude tumor development. As the lymph node disorganization progresses, it is probable that GCs collapse and neoplastic T_{FH} cells are diluted amid large numbers of reactive cells. This scenario is consistent with the histologic data showing hyperplasic expansion of GCs in the nonenlarged lymph nodes leading to complete effacement of the nodal architecture in enlarged tumor lymph nodes.

Tumors from Roquin$^{san/+}$ mice exhibit T-cell clonality

Expansion of 1 or several T-cell clones is a common feature of AITL tumor development.[28-30] We examined clonality of both T and B cells in tumor lymph nodes by PCR amplification of TCR-β and IgH genes, respectively. Clonal rearrangements were found in the TCR-β gene in 12 of 15 cases (Table 2). In contrast, a clonal peak of the IgH gene was found in only 1 case (Table 2). Five cases were also examined for clonal rearrangements in the TCR-γ gene; however, no PCR products were amplified (data not shown).

To determine whether the observed clonality corresponded to expanded T_{FH}-cell clones, we performed additional studies on T_{FH} ($CD4^+CXC5^+PD\text{-}1^{hi}$) and $CD4^+$ non-T_{FH} cells ($CD4^+CXCR5^-PD\text{-}1^{lo}$) purified by flow cytometry. T_{FH} cells from *Roquin*$^{san/+}$ mice with and without tumors were found to be more clonal than T_{FH} cells from *Roquin*$^{+/+}$ mice (Figure 6A; Table 3). Furthermore, T_{FH} cells from *Roquin*$^{san/+}$ mice exhibited a more restricted TCR-βV repertoire with the total number of TCR-βV chains detected in each sample being much less than T_{FH} cells from *Roquin*$^{+/+}$ mice (Table 3).

Of particular interest, T_{FH} cells also exhibited more clonality than $CD4^+$ non-T_{FH} cells from the same lymph nodes (Figure 6B; Table 3). Importantly, the clonal peaks detected in the T_{FH} samples often (68%) composed at least 5% of the total TCR-βV repertoire, and each sample had at least 1 clone that accounted for more than

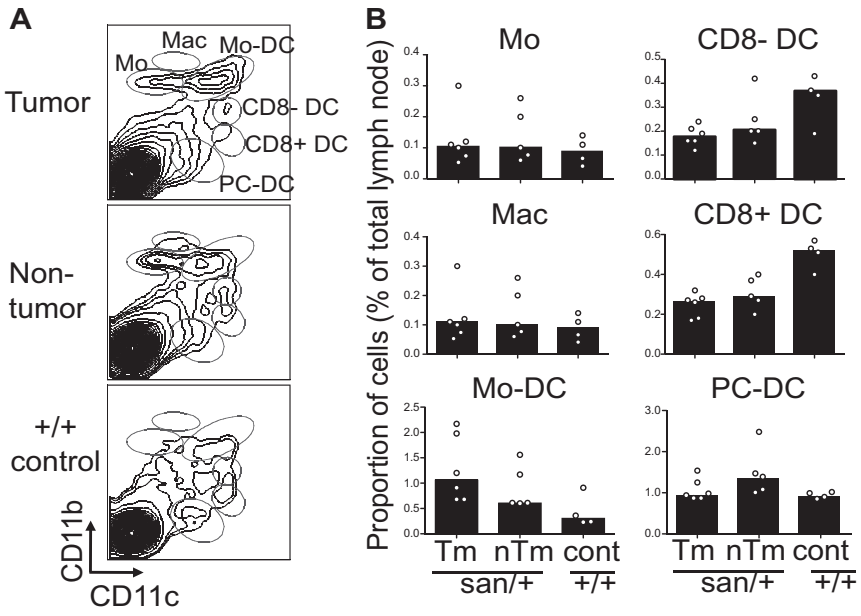

Figure 5. Proportions of myeloid cell populations in tumor lymph nodes from *Roquin*$^{san/+}$ mice. Proportions of myeloid cell populations (monocytes [Mo], macrophages [Mac], monocyte dendritic cells [Mo-DC], CD8$^+$ and CD8$^-$ DCs, and plasmacytoid DCs [PC-DC]) in tumor and nontumor lymph nodes from *Roquin*$^{san/+}$ compared with control *Roquin*$^{+/+}$ mice. (A) Representative FACS plots. (B) Cell numbers of each subset are given as a proportion of total lymph node cells. Histograms represent the median values of 4 to 6 mice 26 to 40 weeks of age. Results are representative of 2 independent experiments.

10% of the repertoire, suggesting that this clone is highly overexpressed. In contrast, in the non-T_{FH} samples, only 19% of clonal peaks had a frequency more than or equal to 5%, and only 1 of 5 samples had a clone that accounted for more than 10% of the repertoire. Together, these data indicate that lymph nodes from *Roquin*$^{san/+}$ mice typically display expanded T_{FH}-cell clones, and this may possibly precede tumor development.

T_{FH} cells drive AITL-like tumors of Roquin$^{san/+}$ mice

To further investigate a possible role of T_{FH} cells in driving or maintaining tumors in *Roquin*$^{san/+}$ mice, we introduced genetic manipulations that reduce the number and/or function of T_{FH} cells, and evaluated the tumor incidence in these mice. Reduction or deficiencies in CD28, SAP, and ICOS[19] have already been shown to decrease the numbers of T_{FH} cells in *Roquin*$^{san/san}$ mice. SAP deficiency in *Roquin*$^{san/san}$ mice results in a 4-fold reduction in T_{FH} cells and abrogates spontaneous GC formation but does not alter T_H1 or T_H2 subsets.[20] CD28 deficiency corrects excessive T_{FH} accumulation in *Roquin*$^{san/san}$ mice to levels comparable with *Roquin*$^{+/+}$ mice.[20] Similarly, ICOS hemizygosity also reduces T_{FH}-cell numbers.[17]

Tumor incidence in *Roquin*$^{san/+}$ mice that were also deficient in *Cd28*, *Sap*, or *Icos* was significantly reduced compared with wild-type *Roquin*$^{san/+}$ mice (Figure 7). Strikingly, mice lacking SAP were completely protected from tumor development. This is particularly significant because, of all 3 molecules, SAP deficiency has the most selective effect on T_{FH}-cell numbers. These results strongly suggest that T_{FH} cells play a crucial role in tumor development and support the idea that neoplastic transformation of T_{FH} cells in *Roquin*$^{san/+}$ mice results in AITL-like disease.

We next asked whether loss of heterozygosity (LOH) within T_{FH} cells so that they only express the mutant form of ROQUIN could explain the occurrence of AITL-like disease in only approximately 50% of *Roquin*$^{san/+}$ mice. To test this, we generated gDNA samples from low numbers of FACS-purified T_{FH} cells (10-100) from tumor and nontumor lymph nodes and investigated LOH using nested PCR. All samples remained heterozygous for the *Roquin*^{san} allele. To exclude the possibility that LOH was occurring in only a subset of T_{FH} cells and thus masked by the pooling of multiple cells, we extended the study to examine LOH in single cells. Although we were able to detect loss of either the *Roquin*^{san} or the *Roquin*$^+$ allele at the single-cell level, this phenonomen was not exclusive to or increased in tumor-derived T_{FH} cells compared with either naive T cells or T_{FH} cells from *Roquin*$^{san/+}$ nontumor controls (data not shown). Thus, we conclude that, although LOH may occur in individual lymphocytes in *Roquin*$^{san/+}$ mice, this is not causally related with the development of AITL-like disease.

Table 2. Summary of clonality of TCR-β receptors in lymph nodes from *Roquin*$^{san/+}$ mice

Case no.	TCR-β					IgH
	V1J1	V1J2	D1J1	D2J2	D1J2	
1406	C	P	P	P	P	P
1407	C	P	P	P	P	C
1413	P	NA	P	P	NA	NA
1418	P	P	C	P	C	P
1420	C	P	P	P	P	P
1423	C	P	P	P	C	P
1424	P	P	P	P	P	P
3225	P	C	P	P	C	P
860	NA	NA	C	NA	NA	NA
39	C	P	C	C	NA	P
83	P	P	NA	NA	NA	P
820	P	P	C	P	P	P
821	C	P	P	P	P	P
824	P	C	P	P	P	P
5593	C	P	C	C	NA	NA

C indicates clonal; P, polyclonal; and NA, not amplified.

Discussion

AITL is an aggressive T-cell malignancy with characteristic autoimmune-like manifestations related to B-cell reactivity that make it a complex disease with no appropriate mouse model to

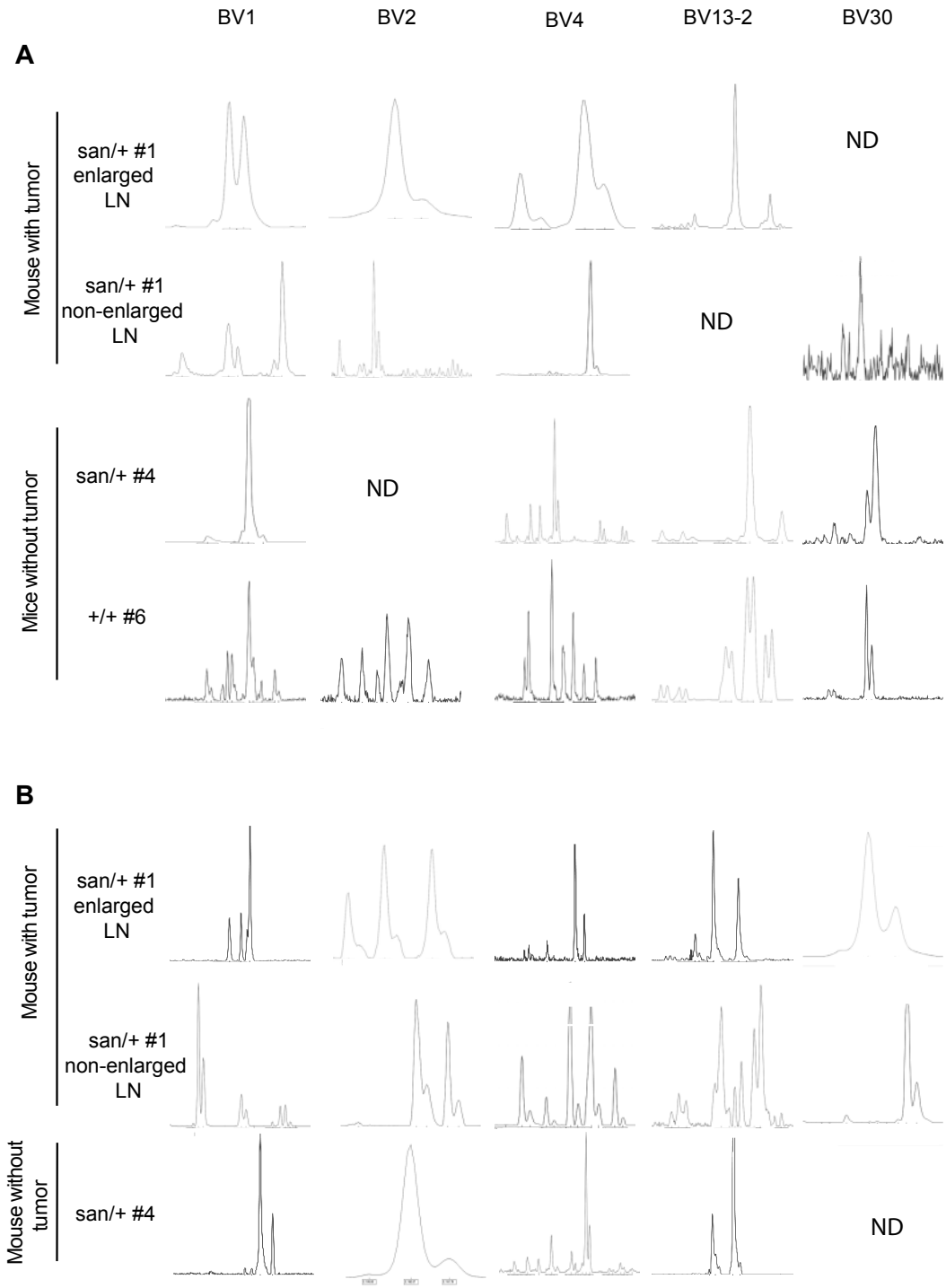

Figure 6. Tumors from *Roquin*$^{san/+}$ mice exhibit T-cell clonality. T_{FH} (A) and non-T_{FH} cells (B) isolated from the lymph nodes of *Roquin*$^{san/+}$ mice with or without tumors and lymph nodes from *Roquin*$^{+/+}$ mice. In mice with tumors, a nonenlarged lymph node was also analyzed for clonality. Cells were purified by flow cytometry. TCRV-β chains were amplified by PCR and clonality determined by CDR3 spectratyping. #Mouse number, as in Table 3. Analysis of non-T_{FH} cells from *Roquin*$^{+/+}$ mice was not performed. Panels show 5 representative TCRV-β chains selected on the basis of those expressed in most samples. ND indicates not detected. All mice were 26 to 40 weeks of age.

date. Here we have described that heterozygosity for *Roquin*^{san} recapitulates most of the clinical, histologic, and cellular features associated with AITL, including lymphadenopathy, hypergammaglobulinemia, increased T_{FH}-cell numbers,[9,10] and clonal expansion of T cells.[28-30] Thus, this work establishes *Roquin*$^{san/+}$ mice as a potentially useful mouse model of this peculiar type of peripheral T-cell lymphoma.

Notably, AITL is characterized by a large histopathologic spectrum with 3 patterns described: hyperplasic GCs and no increase in FDC (pattern 1), depleted follicles and loss of normal lymph node architecture (pattern 2), and complete effacement of lymph node architecture, with prominent FDCs (pattern 3) in full-blown AITL. All 3 patterns display polymorphic infiltrates and vascular proliferation. The majority of patients present with pattern

Table 3. TCR BV clonality and frequency in T_{FH} and non-T_{FH} cells

	T_{FH}														Non-T_{FH}									
	Tumor								Nontumor				Tumor								Nontumor:	
	Enlarged LN						Normal LN						Enlarged LN				Normal LN					
TCR-βV	Mouse 1		Mouse 2		Mouse 3		Mouse 1		Mouse 2		*Roquin*$^{san/+}$ (mouse 4)		Roquin$^{+/+}$ (mouse 6)		Mouse 1		Mouse 5		Mouse 1		Mouse 5		*Roquin*$^{san/+}$ (mouse 4)	
BV1	C	< 1	IN	12	C	22	P	25	C	11	C	15	P	5	P	10	P	2	P	12	O	3	O	4
BV2	C	2	IN	2	NA		P	20	C	< 1	NA		P	5	P	4	NA		O	4	P	11	C	< 1
BV3	O	< 1	NA		O	14	NA		IN	8	NA		P	6	O	3	NA		P	6	NA		C	11
BV4	O	12	O	5	C	9	C	18	O	8	P	< 1	P	3	O	6	NA		P	8	NA		O	5
BV5	NA		NA		O	9	NA		NA		NA		IN	8	NA		P	5	P	11	P	26	NA	
BV12-1	C	7	C	5	NA		NA		O	11	NA		P	5	C	2	O	3	O	1	P	1	NA	
BV12-2	C	1	P	1	NA		C	< 1	C	1	NA		P	1	C	1	O	1	P	1	C	2	IN	13
BV13-1	C	3	NA		NA		NA		NA		O	26	P	6	P	6	O	1	NA		O	3	O	2
BV13-2	C	9	C	12	O	< 1	NA		C	13	C	48	P	10	P	13	P	40	P	9	O	11	O	13
BV13-3	NA		NA		NA		NA		NA		NA		NA	7	P	10	NA		P	8	P	11	NA	
BV14	O	10	P	37	P	10	NA		NA		NA		P	2	P	5	NA		O	2	O	4	C	3
BV15	C	8	IN	2	IN	10	NA		O	4	NA		P	5	O	3	P	5	C	4	O	9	C	1
BV16	P	18	P	6	O	14	NA		P	8	NA		P	9	P	9	P	9	P	5	O	4	O	3
BV17	C	11	NA		NA		NA		C	5	NA		IN	3	C	3	C	1	P	1	C	2	NA	
BV19	NA		O	6	NA		NA		C	12	NA		P	6	C	3	P	10	P	5	C	2	C	14
BV20	O	2	C	< 1	NA		NA		C	3	C	11	IN	3	O	5	C	6	O	2	C	3	C	< 1
BV23	O	10	C	7	NA		NA		NA		NA		O	1	C	1	C	2	C	8	NA		NA	
BV24	NA		NA		NA		NA		NA		NA		NA		NA		NA		NA		NA		NA	
BV26	NA		NA		NA		P	36	IN	5	NA		P	4	C	1	C	2	P	4	O	1	C	7
BV29	NA		C	5	C	7	NA		NA		NA		IN	5	P	3	C	2	P	3	C	1	P	13
BV30	IN	6	NA		NA		P	36	NA		C	< 1	C	1	C	2	NA		C	1	NA		NA	
BV31	NA		NA		C	7	NA		P	12	NA		O	8	O	8	O	10	P	5	O	5	P	12

Values are the percentage of total TCR-βV chain mRNA.

C indicates clonal; O, oligoclonal; P, polyclonal; NA, not amplified (mRNA product not detected); and IN, inconclusive (mRNA detected, but CDR3 spectratyping inconclusive).

2 or 3 (consequently known as classic AITL).[11,31-33] Although these different morphologic variants do not appear to influence survival, progression from pattern 1 to pattern 2 or 3 is well documented, suggesting that pattern 1 is an early phase of the disease.[11,31,32] *Roquin*$^{san/+}$ enlarged lymph nodes, which do not contain hyperplasic GCs, share features with classic AITL (pattern 2 or 3). By contrast, hyperplasic GCs were a frequent feature of contralateral "nontumor" lymph nodes in the same mice, suggesting that these may already be displaying the early form of disease (pattern 1). The proportion of Ki67$^+$ T_{FH} cells increased from *Roquin*$^{+/+}$ to nontumor lymph nodes and again in tumor lymph nodes from the same mouse, suggesting that increased proliferation correlates with tumor development.

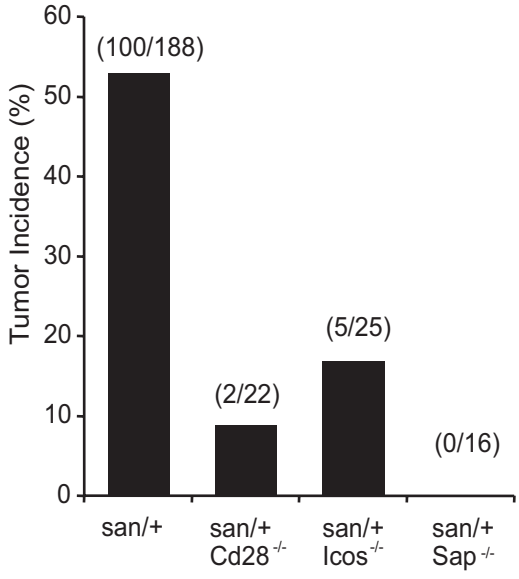

Figure 7. T_{FH} cells are the drivers of tumor development in *Roquin*$^{san/+}$ mice. Incidence of tumors in *Roquin*$^{san/+}$ mice crossed to genetic backgrounds known to reduce T_{FH} cell numbers and function. All mice were 26 to 40 weeks of age.

Attempts to transplant AITL-like tumors were unsuccessful consistent with the reported poor transplantability of most peripheral T-cell tumors and B-cell lymphomas of GC origin.[34-37] The difficulty in transplanting these tumors probably relates to the specialized environment of the GC, containing unique niches and stromal elements that may be required to support tumor growth[1-3] and to the fact that terminally differentiated T_{FH} cells do not recirculate because of the down-regulation of CCR7.[38]

The absence of an expanded FDC network was arguably the one discordant feature between the tumors of *Roquin*$^{san/+}$ mice and AITL. Most AITL patients are infected by EBV, which does not infect mice. It is therefore possible that the FDC expansion is a consequence of EBV infection.[39] Although EBV infection is normally associated with B cells, FDCs express high levels of CD21, the surface receptor for this virus,[40] and EBV infection has been associated with several FDC tumors.[41,42] The role of EBV in FDC expansion in AITL remains to be determined. Alternatively, it is possible that EBV infection and/or FDC expansion in humans may drive/support T_{FH} growth and/or survival, providing the right environment for neoplasia to develop. Indeed, in human AITL samples, neoplastic T cells are intimately associated with FDC networks.[43] In contrast, the cell-autonomous accumulation of T_{FH} cells in the presence of the *Roquin "san"* mutation may bypass the requirement of an expanded FDC network.

Increased clonality among T_{FH} cells compared with non-T_{FH} cells from the same lymph node, even in nontumor lymph nodes from *Roquin*$^{san/+}$ mice, is an intriguing finding. It suggests that ongoing antigen-specific responses to either self or foreign antigens are probably driving expansion of nonmalignant T_{FH} clones, some of which may subsequently become neoplastic, thus mimicking early stages of AITL.

Our data provide experimental evidence in support of the notion emerging from histopathologic studies that T_{FH} cells may be the cellular counterparts of AITL.[9,13,44] Indeed, blockade in T_{FH}-cell development completely prevented AITL-like tumor development. AITL patients do not respond well to cytotoxic chemotherapeutic treatment,[4,5] and alternative strategies are needed to improve patient outcome.[3,6] Novel therapies that neutralize or deplete T_{FH} cells by targeting ICOS, PD-1, SAP, or the PI3K signaling pathway[45,46] may prove to be more specific and effective and improve prognosis. Because AITL neoplastic cells represent only a small proportion of the tumor,[3,7,8,11] conventional T-cell-lymphoma mouse models,[47,48] in which disease is the result of uncontrolled malignant cell proliferation, may not be useful in testing new therapeutic compounds. In contrast, the *Roquin*$^{san/+}$ model of AITL should be useful for preclinical testing of these or other novel therapeutic compounds.

In addition, *Roquin*$^{san/+}$ mice may help further understanding of AITL disease development mechanisms and pathways. Despite all *Roquin*$^{san/+}$ mice exhibiting dysregulated T_{FH} cells, only 53% of mice develop AITL-like disease. This suggests that additional, possibly mutagenic, events are required for neoplastic transformation. Dissecting the pathway(s) that lead to lymphadenopathy and AITL-like disease in *Roquin*$^{san/+}$ mice may thereby provide important insights into human disease development and progression.

Acknowledgments

The authors thank M. Townsend for cryosectioning, A. Prins for histology, Dr H. Vohra and M. Devoy for cell sorting, and Debbie Howard for technical assistance.

This work was supported by a Viertel Senior Medical Research Fellowship and National Health and Medical Research Council program and project grants (C.G.V.) and a National Health and Medical Research Council Overseas Biomedical Fellowship (J.I.E.).

Authorship

Contribution: J.I.E. performed and analyzed experiments and wrote the manuscript; T.C., S.-M.R.-P., J.L.M., X.H., M.N.-G., J.F.G., and S.M.-M. and performed and analyzed experiments; M.-H.D.-L. and P.G. provided critical analysis of the manuscript and clinical interpretation of the data; G.W. designed experiments and interpreted data; M.C.C. helped conceive the original study and had intellectual input; and M.A.P. and C.G.V. conceived the study, analyzed data, provided intellectual input, and revised the manuscript.

Conflict-of-interest disclosure: The authors declare no competing financial interests.

Correspondence: Carola G. Vinuesa, Department of Pathogens and Immunity, John Curtin School of Medical Research, Australian National University, Building 131, Garran Road, Canberra, ACT 0200, Australia; e-mail: carola.vinuesa@anu.edu.au.

References

1. A clinical evaluation of the International Lymphoma Study Group classification of non-Hodgkin's lymphoma: the Non-Hodgkin's Lymphoma Classification Project. *Blood.* 1997;89(11):3909-3918.
2. Ghani AM, Krause JR. Bone marrow biopsy findings in angioimmunoblastic lymphadenopathy. *Br J Haematol.* 1985;61(2):203-213.
3. Mourad N, Mounier N, Briere J, et al. Clinical, biologic, and pathologic features in 157 patients with angioimmunoblastic T-cell lymphoma treated within the Groupe d'Etude des Lymphomes de l'Adulte (GELA) trials. *Blood.* 2008;111(9):4463-4470.
4. Murayama T, Imoto S, Takahashi T, Ito M, Matozaki S, Nakagawa T. Successful treatment of angioimmunoblastic lymphadenopathy with dysproteinemia with cyclosporin A. *Cancer.* 1992;69(10):2567-2570.
5. Takemori N, Kodaira J, Toyoshima N, et al. Successful treatment of immunoblastic lymphadenopathy-like T-cell lymphoma with cyclosporin A. *Leuk Lymphoma.* 1999;35(3):389-395.
6. Lachenal F, Berger F, Ghesquieres H, et al. Angioimmunoblastic T-cell lymphoma: clinical and laboratory features at diagnosis in 77 patients. *Medicine (Baltimore).* 2007;86(5):282-292.
7. Archimbaud E, Coiffier B, Bryon PA, Vasselon C, Brizard CP, Viala JJ. Prognostic factors in angioimmunoblastic lymphadenopathy. *Cancer.* 1987;59(2):208-212.
8. Ch'ang HJ, Su IJ, Chen CL, et al. Angioimmunoblastic lymphadenopathy with dysproteinemia: lack of a prognostic value of clear cell morphology. *Oncology.* 1997;54(3):193-198.
9. de Leval L, Rickman DS, Thielen C, et al. The gene expression profile of nodal peripheral T-cell lymphoma demonstrates a molecular link between angioimmunoblastic T-cell lymphoma (AITL) and follicular helper T (TFH) cells. *Blood.* 2007;109(11):4952-4963.
10. Piccaluga PP, Agostinelli C, Califano A, et al. Gene expression analysis of angioimmunoblastic lymphoma indicates derivation from T follicular helper cells and vascular endothelial growth factor deregulation. *Cancer Res.* 2007;67(22):10703-10710.
11. Attygalle A, Al-Jehani R, Diss TC, et al. Neoplastic T cells in angioimmunoblastic T-cell lymphoma express CD10. *Blood.* 2002;99(2):627-633.
12. Dorfman DM, Brown JA, Shahsafaei A, Freeman GJ. Programmed death-1 (PD-1) is a marker of germinal center-associated T cells and angioimmunoblastic T-cell lymphoma. *Am J Surg Pathol.* 2006;30(7):802-810.
13. Dupuis J, Boye K, Martin N, et al. Expression of CXCL13 by neoplastic cells in angioimmunoblastic T-cell lymphoma (AITL): a new diagnostic marker providing evidence that AITL derives from follicular helper T cells. *Am J Surg Pathol.* 2006;30(4):490-494.
14. Marafioti T, Paterson JC, Ballabio E, et al. The inducible T-cell co-stimulator molecule is expressed on subsets of T cells and is a new marker of lymphomas of T follicular helper cell-derivation. *Haematologica.* 2010;95(3):432-439.
15. Vinuesa CG, Cook MC, Angelucci C, et al. A RING-type ubiquitin ligase family member required to repress follicular helper T cells and autoimmunity. *Nature.* 2005;435(7041):452-458.
16. Glasmacher E, Hoefig KP, Vogel KU, et al. Roquin binds inducible costimulator mRNA and effectors of mRNA decay to induce microRNA-independent post-transcriptional repression. *Nat Immunol.* 2010;11(8):725-733.
17. Yu D, Tan AH, Hu X, et al. Roquin represses autoimmunity by limiting inducible T-cell co-stimulator messenger RNA. *Nature.* 2007;450(7167):299-303.
18. Athanasopoulos V, Barker A, Yu D, et al. The ROQUIN family of proteins localizes to stress granules via the ROQ domain and binds target mRNAs. *FEBS J.* 2010;277(9):2109-2127.
19. Linterman MA, Rigby RJ, Wong R, et al. Roquin differentiates the specialized functions of duplicated T cell costimulatory receptor genes CD28 and ICOS. *Immunity.* 2009;30(2):228-241.
20. Linterman MA, Rigby RJ, Wong RK, et al. Follicular helper T cells are required for systemic autoimmunity. *J Exp Med.* 2009;206(3):561-576.
21. Canela A, Martin-Caballero J, Flores JM, Blasco MA. Constitutive expression of tert in thymocytes leads to increased incidence and dissemination of T-cell lymphoma in Lck-Tert mice. *Mol Cell Biol.* 2004;24(10):4275-4293.
22. Gärtner F, Alt FW, Monroe R, et al. Immature thymocytes employ distinct signaling pathways for allelic exclusion versus differentiation and expansion. *Immunity.* 1999;10(5):537-546.
23. Kawamoto H, Ikawa T, Ohmura K, Fujimoto S, Katsura Y. T cell progenitors emerge earlier than B cell progenitors in the murine fetal liver. *Immunity.* 2000;12(4):441-450.
24. van Dongen JJ, Langerak AW, Bruggemann M, et al. Design and standardization of PCR primers and protocols for detection of clonal immunoglobulin and T-cell receptor gene recombinations in suspect lymphoproliferations: report of the BIOMED-2 Concerted Action BMH4-CT98-3936. *Leukemia.* 2003;17(12):2257-2317.

25. Greer JP. Therapy of peripheral T/NK neoplasms. *Hematology Am Soc Hematol Educ Program.* 2006;2006:331-337.
26. Jaffe ES. Pathobiology of peripheral T-cell lymphomas. *Hematology Am Soc Hematol Educ Program.* 2006;2006:317-322.
27. Lachenal F. [Angioimmunoblastic T-cell lymphoma]. *Presse Med.* 2007;36(11):1655-1662.
28. Lipford EH, Smith HR, Pittaluga S, Jaffe ES, Steinberg AD, Cossman J. Clonality of angioimmunoblastic lymphadenopathy and implications for its evolution to malignant lymphoma. *J Clin Invest.* 1987;79(2):637-642.
29. O'Connor NT, Crick JA, Wainscoat JS, et al. Evidence for monoclonal T lymphocyte proliferation in angioimmunoblastic lymphadenopathy. *J Clin Pathol.* 1986;39(11):1229-1232.
30. Weiss LM, Strickler JG, Dorfman RF, Horning SJ, Warnke RA, Sklar J. Clonal T-cell populations in angioimmunoblastic lymphadenopathy and angioimmunoblastic lymphadenopathy-like lymphoma. *Am J Pathol.* 1986;122(3):392-397.
31. Attygalle AD, Kyriakou C, Dupuis J, et al. Histologic evolution of angioimmunoblastic T-cell lymphoma in consecutive biopsies: clinical correlation and insights into natural history and disease progression. *Am J Surg Pathol.* 2007;31(7):1077-1088.
32. Rodriguez-Justo M, Attygalle AD, Munson P, Roncador G, Marafioti T, Piris MA. Angioimmunoblastic T-cell lymphoma with hyperplastic germinal centres: a neoplasia with origin in the outer zone of the germinal centre? Clinicopathological and immunohistochemical study of 10 cases with follicular T-cell markers. *Mod Pathol.* 2009;22(6):753-761.
33. Dogan A, Gaulard P, Jaffe ES, et al. Angioimmunoblastic T-cell lymphoma. In: Swerdlow SH, Campo E, Harris NL, et al, eds. *Pathology and Genetics of Tumours of Haematopetic and Lymphoid Tissues*: *World Health Organisation Classification of Tumours.* Lyon, France: IARC Press; 2008:309-311.
34. Saito M, Gao J, Basso K, et al. A signaling pathway mediating downregulation of BCL6 in germinal center B cells is blocked by BCL6 gene alterations in B cell lymphoma. *Cancer Cell.* 2007;12(3):280-292.
35. Zhou P, Levy NB, Xie H, et al. MCL1 transgenic mice exhibit a high incidence of B-cell lymphoma manifested as a spectrum of histologic subtypes. *Blood.* 2001;97(12):3902-3909.
36. Ranger AM, Zha J, Harada H, et al. Bad-deficient mice develop diffuse large B cell lymphoma. *Proc Natl Acad Sci U S A.* 2003;100(16):9324-9329.
37. Egle A, Harris AW, Bath ML, O'Reilly L, Cory S. VavP-Bcl2 transgenic mice develop follicular lymphoma preceded by germinal center hyperplasia. *Blood.* 2004;103(6):2276-2283.
38. Vinuesa CG, Cyster JG. How T cells earn the follicular rite of passage. *Immunity.* 2011;35(5):671-680.
39. Weiss LM, Jaffe ES, Liu XF, Chen YY, Shibata D, Medeiros LJ. Detection and localization of Epstein-Barr viral genomes in angioimmunoblastic lymphadenopathy and angioimmunoblastic lymphadenopathy-like lymphoma. *Blood.* 1992;79(7):1789-1795.
40. Lindhout E, Lakeman A, Mevissen ML, de Groot C. Functionally active Epstein-Barr virus-transformed follicular dendritic cell-like cell lines. *J Exp Med.* 1994;179(4):1173-1184.
41. Cheuk W, Chan JK, Shek TW, et al. Inflammatory pseudotumor-like follicular dendritic cell tumor: a distinctive low-grade malignant intra-abdominal neoplasm with consistent Epstein-Barr virus association. *Am J Surg Pathol.* 2001;25(6):721-731.
42. Laurent C, Meggetto F, de Paiva GR, et al. Follicular dendritic cell tumor of the spleen associated with diffuse large B-cell lymphoma. *Hum Pathol.* 2008;39(5):776-780.
43. Dogan A, Attygalle AD, Kyriakou C. Angioimmunoblastic T-cell lymphoma. *Br J Haematol.* 2003;121(5):681-691.
44. Rodríguez-Pinilla SM, Atienza L, Murillo C, et al. Peripheral T-cell lymphoma with follicular T-cell markers. *Am J Surg Pathol.* 2008;32(12):1787-1799.
45. Rolf J, Bell SE, Kovesdi D, et al. Phosphoinositide 3-kinase activity in T cells regulates the magnitude of the germinal center reaction. *J Immunol.* 2010;185(7):4042-4052.
46. Rolf J, Fairfax K, Turner M. Signaling pathways in T follicular helper cells. *J Immunol.* 2010;184(12):6563-6568.
47. Li GC, Ouyang H, Li X, et al. Ku70: a candidate tumor suppressor gene for murine T cell lymphoma. *Mol Cell.* 1998;2(1):1-8.
48. Pfeifer W, Levi E, Petrogiannis-Haliotis T, Lehmann L, Wang Z, Kadin ME. A murine xenograft model for human CD30+ anaplastic large cell lymphoma: successful growth inhibition with an anti-CD30 antibody (HeFi-1). *Am J Pathol.* 1999;155(4):1353-1359.